

Model of Soil-structure Interaction of Objects Resting on Finite Depth Soil Layers for Seismic Design

Zsuzsa B. Pap^{1*}, László P. Kollár¹

¹ Department of Structural Engineering, Faculty of Civil Engineering, Budapest University of Technology and Economics, H-1111 Budapest, Műegyetem rkp. 3., Hungary

* Corresponding author, e-mail: pap.zsuzsa@epito.bme.hu

Received: 27 May 2019, Accepted: 24 October 2019, Published online: 10 December 2019

Abstract

In case of seismic design of structures the deformability and damping of the soil should be considered, which can be performed in several ways. The infinite soil half space can be approximated with the cone model, which gives constant values for the spring stiffnesses and dashpot characteristics, and an additional mass element for rocking motion. To approximate the dynamic impedance function of a soil layer more complex models were also applied. Most of the methods do not take into account the finite dimensions of the soil, which results significantly different behavior than spring-dashpot systems. To consider the effect of a finite layer a new simple model based on a physical approach is given for the horizontal excitation of strip foundations. Numerical verification is presented, and the parameter range is determined, where the application of the new model is recommended, since applying a spring-dashpot model results in significant errors.

Keywords

soil-structure interaction, horizontal excitation, simplified model, finite soil layer

1 Introduction

In case of earthquake resistant design the effect of the soil must be taken into account. The soil influences the response of the structure in different ways [1]. The deformation of the soil can be taken into account by spring elements, however for dynamic analysis it is inaccurate [2]. The most exact method is the direct approach (Fig. 1(a)), where the structure and part of the soil is modelled together, although it can be very time consuming and may need significant computation effort. In linear cases the soil layer can be represented by an impedance function, which is the ratio of harmonic force on the weightless foundation and the steady state response of the soil layer as a function of the exciting frequency. The development of the impedance function is summarized in the excellent review paper of Kausel [3]. The impedance function can be interpreted as a frequency dependent spring and dashpot element (Fig. 1(b)). Its applicability is rather complicated in time domain, therefore to simplify the procedure, the frequency dependent characteristics are often approximated by constant values in practical design [4], a spring and dashpot is used for every direction (Fig. 1(c)). (In the article only the horizontal direction will be analyzed.)

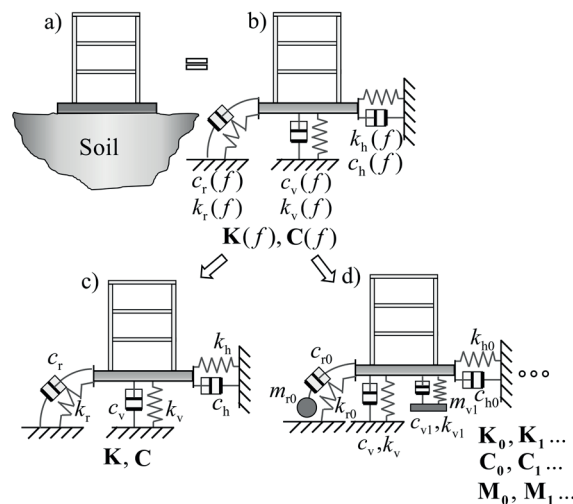


Fig. 1 The modelling levels of soil effect: a) direct approach, b) impedance function, c) one, frequency independent spring and dashpot element for all directions, d) more complex lumped models

The simple spring-dashpot system (with constant characteristics) can be applicable in those cases, when the soil is infinite [4], but also for this case neglecting the frequency dependency may cause significant errors [5, 6]. When the vertical dimension of the soil is finite the error

can be substantially higher [7, 8]. The range in which the response of a soil layer and a spring-dashpot model is significantly different is investigated in [2].

The infinite soil half space can be approximated with the cone model (Fig. 2(a)), which gives constant values for the spring stiffnesses and dashpot characteristics, and an additional mass element for rocking motion [4]. To approximate the dynamic impedance function of a soil layer more complex models were also applied (Fig. 1(d)). Meek and Wolf used a layered cone model and developed echo constants to take into account the effect of the refracted waves [9]. Wolf also developed more complex lumped parameter models for the different excitations (for example Fig. 2(b)) [10–13]. In these cases, the parameters are calculated with the least square method to approximate properly the exact impedance function. Saitoh also constructed a more complex lumped model with frequency independent parameters and suggested a new element type [14]. The more complex model is used, the better accuracy can be reached (Fig. 2(b)) [6].

Recently we investigated the effect of resonance in case of finite soil depth [2] by FE calculations, and the impedance curves were determined. Rigid objects subjected to both horizontal and rocking excitation were examined, and it was found that the phase angles between the applied force (or moment) and the displacement (or rotation) for lower frequencies are close to 180 degrees (which means low energy dissipation), while for higher frequencies they are around 90 degrees (which means high energy dissipation). When we compare them to the impedance curves

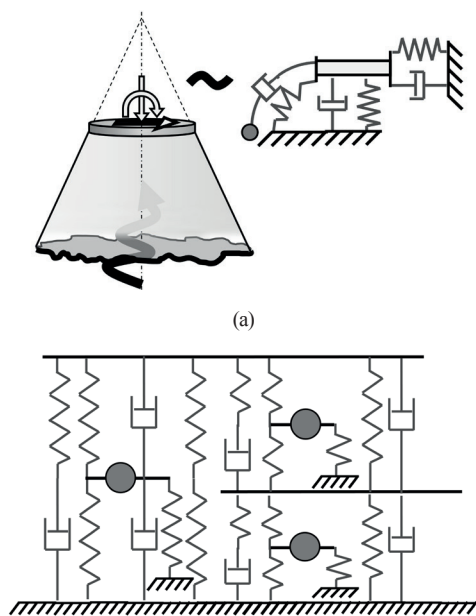


Fig. 2 a) Cone model [4], b) lumped parameter model [13]

of simple spring-dashpot systems the differences in the amplitudes and phase angles can be quite severe, which means that the energy dissipation of the two systems are rather different. Fig. 3 shows the impedance curves in case of direct approach and simplified spring-dashpot model [2], where c and k is calculated as given in [15].

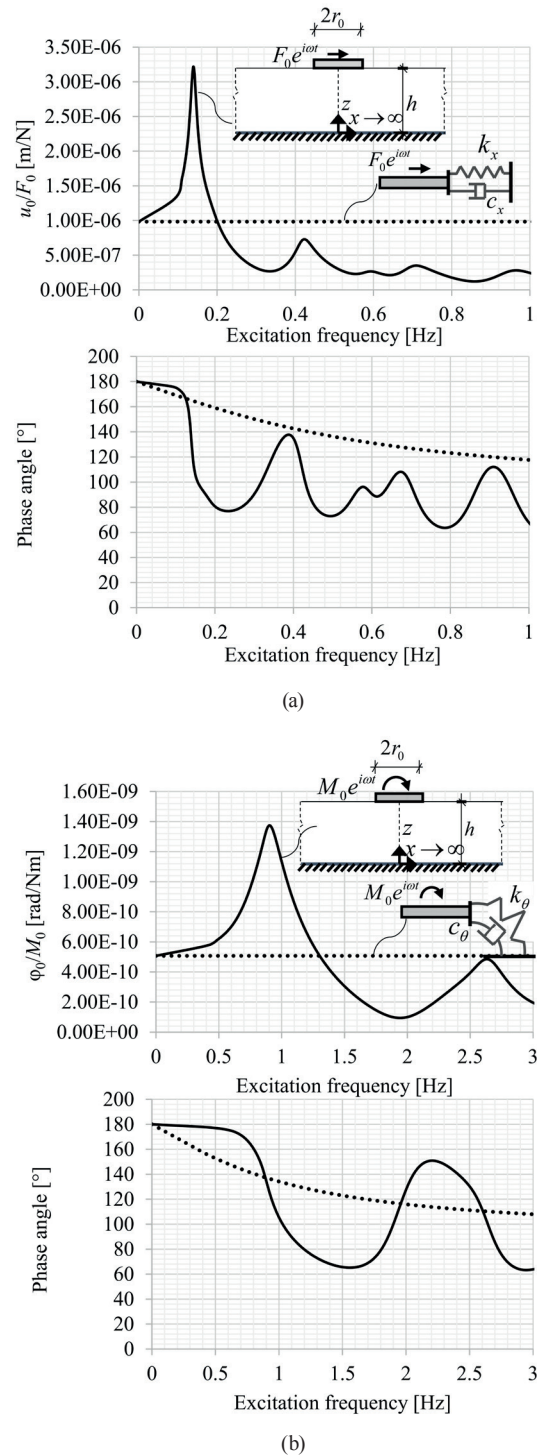


Fig. 3 Comparison of the impedance functions of direct and simplified spring-dashpot models [2], a) horizontal excitation, b) rocking excitation

The above findings were the mayor motivation of this paper and we decided to develop a physically justified simple model, which is capable to explain and numerically capture these phenomena. To put it another way, our aim is to develop a simple model, which shows low energy dissipation under a certain frequency and significantly higher above that value.

2 Problem statement

A rigid object resting on the surface of the ground is considered. The object is infinite in one (y) direction (e.g. strip foundation). The dimension of the soil in the vertical direction is finite, the height is denoted by h while it can be infinite or finite (l) in the x direction (Fig. 4). The rock under the soil is excited by earthquakes on lines $z = 0$ and $x = \pm l/2$. The slip between the rigid foundation and the soil layer and between the soil and the rock is neglected.

We wish:

- to understand the response of the structure including the possible resonance and the overlap with the so called cut-off frequency [10],
- to develop a simplified model which can follow the above phenomena (resonance, effect of the cut-off frequency) by reasonable accuracy,
- to analyze under which circumstances these phenomena occur in case of real structures.

In this article the analyses are limited to 2D problems, and for flat objects undergoes dominantly horizontal motion. Note however, as presented in the Introduction [2] rocking structures on finite soil layer behaves similarly.

In the following sections it will be assumed that the soil behaves in a linearly elastic manner, which will enable us to develop a simple model; but it is noted that the introduced phenomena are important for more realistic soil models as well.

3 Approach

To analyze the 2D problem (Fig. 4) commercially available FE programs (e.g. ANSYS) or analytical tools, or approximate solutions e.g. the Rayleigh-Ritz method can be used.

To analyze the effect of an earthquake both the direct method (time-history analysis), and the harmonic analysis can be applied. (In the latter case the rock is excited by sine waves).

The FE method will be used for the analysis of the 2D problem (Fig. 5(a)), while the Rayleigh-Ritz method to reach an approximate solution (Fig. 5(b)) of the 2D problem, and to derive a simplified (1D) model (Fig. 5(c)). The

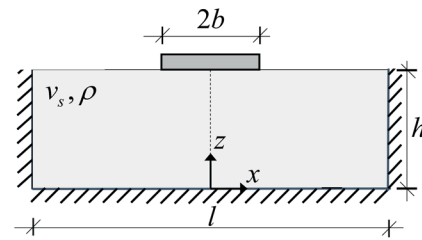


Fig. 4 The analyzed 2D problem with a finite soil layer and a strip foundation

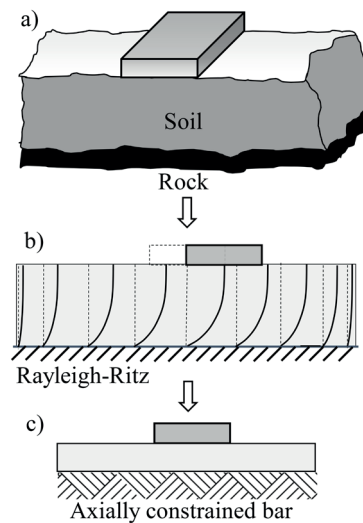


Fig. 5 Methods of analysis: a) Reality, b) approximate solution (Rayleigh-Ritz), c) Solution of a simplified model

latter one will be analyzed by directly solving its differential equation (DE). The results of our approximate model will be verified by 2D FE analyses (direct approach).

As will be shown in this paper, this model of an axially constrained bar (containing a few parameters only) is capable to capture the basic behavior of structures resting on finite depth soil layers.

4 Horizontal excitation of rigid structures on a finite soil layer

To obtain a simplified model (Fig. 5(c)) first the case, when there is no object on the soil (Subsection 4.1) is considered. Then it is extended, and an object with finite size is also taken into account (Subsection 4.2). The solutions and verifications of the model are given in Subsection 4.3.

4.1 Soil layer without an object

The equations of a layer (under plane strain condition) are summarized in Table 1 [16]. In the last row the total mechanical energy of the system is given. According to the Rayleigh-Ritz method the displacement field (for zero Poisson's ratio, $\nu = 0$) is assumed in the following form:

$$u_{2D}(x, z, t) = u(x, t) \sin\left(\frac{\pi z}{2h}\right), \quad (1)$$

where $u(x, t)$ is the displacement function in the x direction and h is the thickness of the soil layer.

Substituting Eq. (1) into the last row of Table 1, after straightforward mathematical manipulations we obtain (assuming $v_{2D}(x, z, t) = 0$):

$$\Pi(u(x, t)) = \frac{Gh}{2} \int_x \left(\frac{du}{dx}\right)^2 dx + \frac{G\pi^2}{16h} \int_x u^2 dx - \frac{\rho h}{4} \int_x \left(\frac{du}{dt}\right)^2 dx, \quad (2)$$

where G is the shear modulus ($G = \rho v_s^2$, v_s is the shear wave velocity), h is the thickness and ρ is the density of the soil layer.

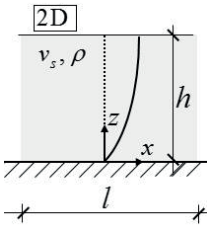
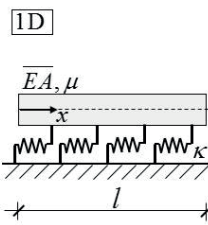
The differential equation of the problem can be derived mathematically as the Euler-Lagrange equation of the stationary condition $\Pi = \text{stac.}$ (see Eq. (2)). The derivation is given in Appendix A, the result is given in the second column of Table 2.

Table 1 Energy and parameters of a 2D soil layer ($v = 0$)

Load	Displacement	Stiffness matrix	Operator
$\mathbf{p} = \begin{bmatrix} p_x(x, z) \\ p_z(x, z) \end{bmatrix}$	$\mathbf{u} = \begin{bmatrix} u_{2D}(x, z, t) \\ v_{2D}(x, z, t) \end{bmatrix}$	$\mathbf{D} = E \begin{bmatrix} 1 & 0 & 0 \\ 0 & 1 & 0 \\ 0 & 0 & \frac{1}{2} \end{bmatrix}$	$\mathbf{L} = \begin{bmatrix} \frac{\partial}{\partial x} & 0 \\ 0 & \frac{\partial}{\partial z} \\ \frac{\partial}{\partial z} & \frac{\partial}{\partial x} \end{bmatrix}$
Energy: $\Pi(u, t) = \frac{1}{2} \int_A (\mathbf{L}\mathbf{u})^T \mathbf{D}(\mathbf{L}\mathbf{u}) dA - \int_A \mathbf{u}^T \mathbf{p} dA + \frac{1}{2} \int_A \rho \left(\frac{\partial \mathbf{u}}{\partial t}\right)^2 dA$			

E : elastic modulus, h : thickness, ρ : density

Table 2 The differential equation and natural circular frequency of the 2D system and the simplified model ($G = \rho v_s^2$)

	2D	1D
		
Diff. equation	$-Ghu'' + \frac{G\pi^2}{8h}u + \frac{\rho h}{2}\ddot{u} = 0$	$-EAu'' + \kappa u + \mu\ddot{u} = 0$
Natural frequency	$\omega_n^2 = \frac{2G\pi^2}{\rho} \left(\frac{1}{8h^2} + \frac{1}{l^2} \right)$	$\omega_n^2 = \frac{\kappa + EA \frac{\pi^2}{l^2}}{\mu}$
Parameters	$EA = Gh; \kappa = \frac{G\pi^2}{8h}; \mu = \frac{\rho h}{2}$	

Now we recall [17] that the DE of a bar with continuous elastic support in the direction of the bar axis is as follows:

$$-EAu'' + \kappa u + \mu\ddot{u} = 0, \quad (3)$$

where EA is the normal stiffness of the bar, κ is the stiffness of the elastic foundation and μ is the mass per unit length of the bar. It may be observed that this equation is equivalent to the DE of the approximation of the 2D problem (Table 2) provided that:

$$EA = Gh; \kappa = \frac{G\pi^2}{8h}; \mu = \frac{\rho h}{2}. \quad (4)$$

With these replacements the natural frequency of an axially constrained bar is identical to that of the soil layer.

4.2 Soil layer with an object

Now we investigate the problem when there is an object on the top of the layer with a total mass of $2m$. First we consider the case when $2b \ll h$ (approximately $b < 5h$, as it will be shown later, see in Fig. 14), i.e. the foundation width is negligible. For this case we may consider only the half of the problem, as shown in Fig. 6(b): the simplified model is a half infinite bar, with a concentrated mass (m) at the end. When the size $2b$ is finite Rayleigh's method must be reconsidered. We assume that the displacement field is uniform with respect to x , under the object:

$$u(x, z, t) = u(b, z, t) \text{ if } 0 \leq x \leq b. \quad (5)$$

Introducing Eq. (5) into the expression of the potential energy (Eq. (2)), and determining the Euler-Lagrange equation, we obtain an axially constrained bar, however there is a replacement spring and mass at the end (Fig. 6(c)):

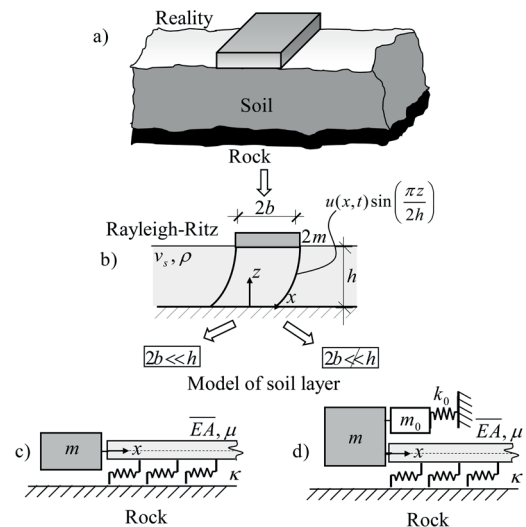


Fig. 6 Simplified models of a soil layer with an object

$$k_0 = \frac{G\pi^2 b}{8h}, \tag{6}$$

$$m_0 = \frac{\rho h}{2} b, \tag{7}$$

both are proportional to the size b .

This model will be verified in the next sections.

4.3 Solution of the simplified model and its verification

To understand the behavior of the soil structure interaction for horizontal excitation the simplified models shown in Fig. 6 will be investigated. First, we summarize the results of the literature for infinite bar with and without elastic foundation.

When an infinite bar is subjected to a half sine pulse displacement at the end, the pulse will travel on the bar with a speed of $c = \sqrt{EA/\mu}$ (see Fig. 7(a)). If the end is subjected to a harmonic excitation the front of the waves will travel with the same speed, c (Fig. 7(b)). It can be shown that the behavior of the bar excited at the end is analogous to the response of a simple dashpot, where the damping coefficient is calculated as $C = \mu c$. The steady-state solution of the bar (or dashpot) subjected to harmonic excitation as a function of the circular frequency (called impedance function) is shown in Fig. 8. On the top we show u_0/F_0 , where u_0 is the amplitude of the applied harmonic displacement and F_0 is the amplitude of the steady-state, harmonic force at the end.

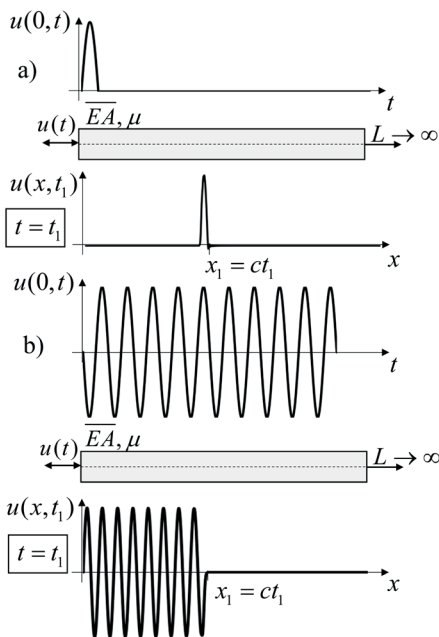


Fig. 7 Behavior of an infinite bar: a) for a half sine pulse, b) for a harmonic excitation

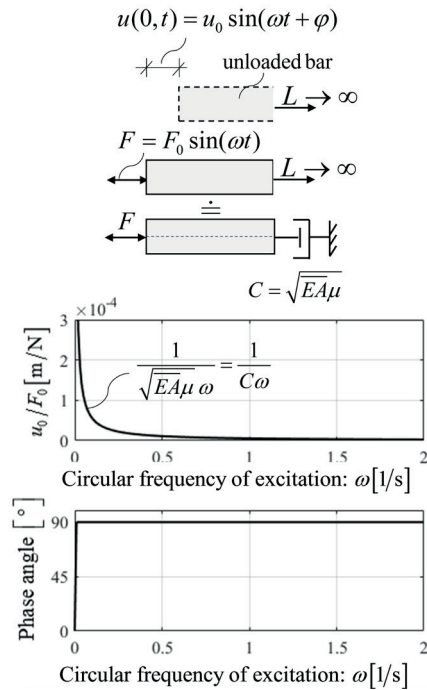


Fig. 8 Impedance of an infinite bar (equivalent to the impedance of a dashpot)

The phase angle between the force and the displacement is $\phi = 90^\circ$, i.e. there is an energy dissipation in the system. (This is called radiation damping.)

When the bar is resting on an elastic foundation the response for harmonic excitation depends on the stiffness of the foundation, or for a given foundation on the frequency of the end displacement. The cut-off frequency [17] is defined as:

$$\omega_c = \sqrt{\frac{\kappa}{\mu}}. \tag{8}$$

When the frequency of excitation is above the cut-off frequency, $\omega > \omega_c$, the bar behaves similarly as a bar without foundation (Fig. 9(a)), but the speed of the front is: $c_p = c/\sqrt{1 - \omega_c^2/\omega^2}$.

When $\omega < \omega_c$ the behavior changes considerably. For this case, even for an excitation, which is applied infinitely long, only a finite length of the bar will be affected, as shown in Fig. 9(b).

In Fig. 10 the steady-state solution is given as a function of the frequency ω . For $\omega > \omega_c$ the phase angle is $\phi = 90^\circ$, and there is an energy dissipation, while for $\omega < \omega_c$, $\phi = 0^\circ$, and there is no energy dissipation. Note that at $\omega = \omega_c$ the response is singular.

For latter use we give the solution for a weightless bar (Fig. 11). The differential equation simplifies to $EAu'' - \kappa u = 0$. Its displacement for an end load $F(t)$ is:

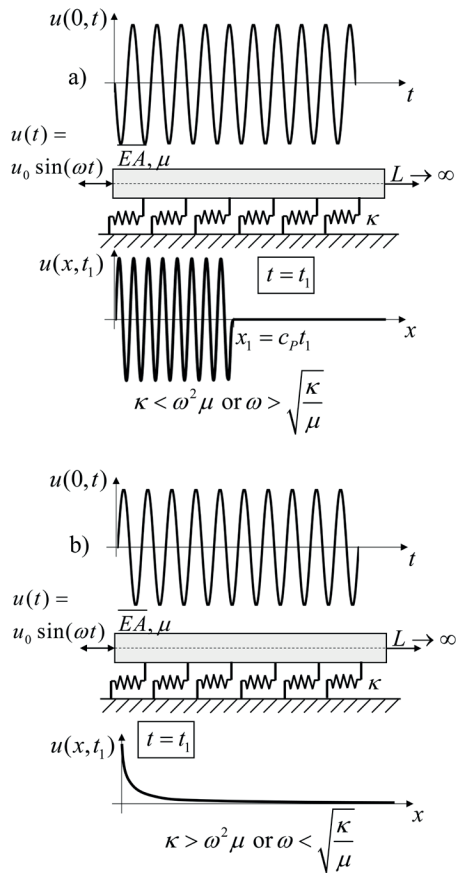


Fig. 9 Behavior of an axially constrained infinite bar: a) $\kappa < \omega^2 \mu$, b) $\kappa > \omega^2 \mu$

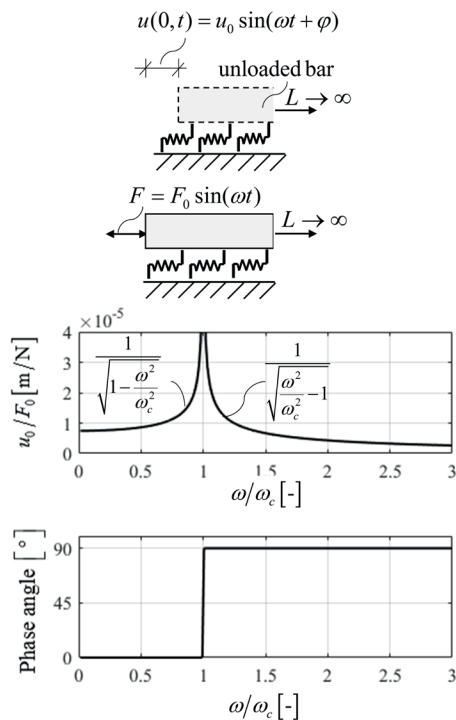


Fig. 10 Impedance of an axially constrained infinite bar (ω is the excitation frequency and $\omega_c = \sqrt{\kappa/\mu}$ is the cut-off frequency)

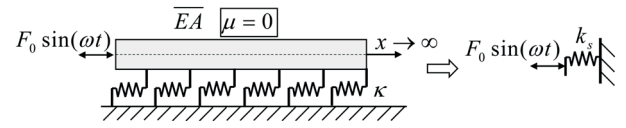


Fig. 11 Equivalent model of a weightless axially constrained infinite bar

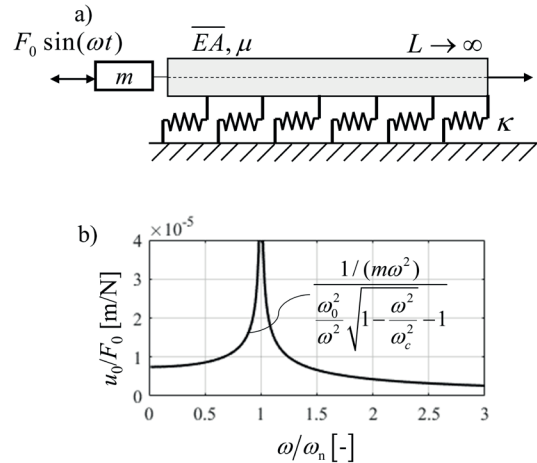


Fig. 12 Infinite bar on an elastic foundation with an end mass (a) and the corresponding impedance curve (b)

$$u(x, t) = \frac{F(t)}{\sqrt{\kappa EA}} e^{-x\sqrt{\kappa/EA}}, \quad u(0, t) = \frac{F(t)}{\sqrt{\kappa EA}}. \quad (9)$$

The second expression is equivalent to the response of a spring with the replacement spring constant:

$$k_s = \sqrt{\kappa EA}. \quad (10)$$

4.3.1 Solution of the model – small foundation size ($2b \ll h$)

Now we consider the model shown in Fig. 6(b), which is subjected to a harmonic force excitation (Fig. 12(a)). The differential equation is given by Eq. (3), the mass and force must be taken into account in the boundary conditions. Although the solution requires some mathematical background, it can be obtained in a straightforward manner (Appendix B). We derived the *steady-state solution* as:

$$u = \bar{D} e^{i(kx - \omega t)}, \quad (11)$$

where $k = \omega \sqrt{\frac{\mu}{EA} \left(1 - \frac{\kappa}{\mu \omega^2} \right)}$ is the wave number, and \bar{D} is:

$$\bar{D} = u(x = 0, \omega) = \frac{F_0 / (m\omega^2)}{\frac{\omega_0^2}{\omega^2} \sqrt{1 - \frac{\omega^2}{\omega_c^2} - 1}}, \quad (12)$$

where ω_c is the cut-off frequency (Eq. (8)) and ω_0 is defined as:

$$\omega_0 = \sqrt{k_s/m}. \tag{13}$$

The natural frequency of the system is obtained from the condition that the denominator of \bar{D} (Eq. (12)) is zero, which results in:

$$\omega_n = \omega_0 \sqrt{\sqrt{1 + \left(\frac{\omega_0^2}{2\omega_c^2}\right)^2} - \frac{\omega_0^2}{2\omega_c^2}}. \tag{14}$$

The corresponding impedance curve is (Fig. 12(b)):

$$Z_0 = \frac{1/(m\omega^2)}{\frac{\omega_0^2}{\omega^2} \sqrt{1 - \frac{\omega^2}{\omega_c^2}} - 1}, \text{ if } \omega < \omega_c \tag{15}$$

$$Z_0 = \frac{1/(m\omega^2)}{\frac{\omega_0^2}{\omega^2} \sqrt{\frac{\omega^2}{\omega_c^2} - 1} + 1}, \text{ if } \omega > \omega_c$$

The transient solution is:

$$u(x=0, t) = \bar{A} \sin(\omega_n t) + \bar{B} \cos(\omega_n t), \tag{16}$$

where ω_n is the natural circular frequency of the system and the constants \bar{A} and \bar{B} are the following:

$$\bar{A} = \frac{v_0 - \omega \bar{D}}{\omega_n}, \quad \bar{B} = u_0. \tag{17}$$

Here u_0 and v_0 are the displacement and velocity of the bar end at $t = 0$.

Now a simplified expression is also presented for the natural frequency with Dunkerly's expression [18]:

$$\frac{1}{\omega_n^2} \approx \frac{1}{\omega_1^2} + \frac{1}{\omega_2^2}, \tag{18}$$

where ω_1 is the natural frequency when m is equal to zero i.e. $\omega_1 = \omega_c$, while ω_2 is the natural frequency of a weightless bar ($\mu = 0$) with a mass at the end. Since the replacement spring constant for $\mu = 0$ is k_s (Eq. (10)), we have $\omega_2 = \omega_0$ (see Eq. (13)).

Eq. (18) results in:

$$\omega_n \approx \sqrt{\frac{1}{\frac{1}{\omega_c^2} + \frac{1}{\omega_0^2}}} = \sqrt{\frac{\omega_c^2 \omega_0^2}{\omega_0^2 + \omega_c^2}}. \tag{19}$$

To verify the derived expressions and to investigate the accuracy of Dunkerly's approach for three different masses the first natural frequencies were calculated by Eqs. (14) and (19), and also by finite element analysis (ANSYS). The results are shown in Table 3.

It can be observed that the analytical and numerical solutions are practically identical, and Dunkerly's approach underestimates the natural frequency.

Now we consider the case when the system is subjected to a harmonic base excitation (Fig. 13). The differential equation (Eq. (3)) will be slightly different:

$$-EAu_r'' + \kappa u_r + \mu \ddot{u}_r = u_{g0} \sin(\omega t), \tag{20}$$

where u_{g0} is the amplitude of base excitation, and u_r is the relative displacement. The amplitude of the steady-state solution ($u_r = \bar{D}_r e^{i(kx - \omega t)}$) can be derived similarly as Eq. (12) and is given below:

$$\bar{D}_r = u_r(x=0, \omega) = \left(\frac{1}{\frac{\omega_0^2}{\omega^2} \sqrt{1 - \frac{\omega^2}{\omega_c^2}} - 1} + 1 \right) u_{g0} \frac{1}{1 - \frac{\omega^2}{\omega_c^2}}. \tag{21}$$

4.3.2 Solution of the model – not negligible foundation size $2b \ll h$

As we stated in Subsection 4.2. (Fig. 6) the only difference between the two models that in the second one at the bar end an equivalent mass and spring defined by Eqs. (6) and (7) must be considered. As a consequence, the differential equations presented in Subsection 4.3.1 are valid, only the boundary conditions must be modified. Without giving the mathematical details of the derivation the amplitude of the steady-state solution ($u = \bar{D}_\kappa e^{i(kx - \omega t)}$) for force excitation is:

Table 3 Comparison of the natural frequencies calculated by Eqs. (14) and (19), and finite element analysis

Mass (t)	Natural frequency f [1/s]			Error of Dunkerly's approach [%]
	Analytical	Numerical	Dunkerly's approximation	
1800	0.406	0.408	0.364	12
9000	0.224	0.225	0.214	5.2
18000	0.163	0.164	0.159	3.1

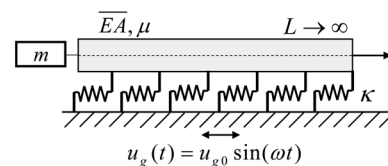


Fig. 13 Base excitation of the system

$$\bar{D}_\kappa = \frac{F_0 / \omega^2 (m + m_0)}{\frac{\omega_{02}^2}{\omega^2} \sqrt{1 - \frac{\omega^2}{\omega_c^2}} - 1 + \frac{\omega_{03}^2}{\omega^2}}, \quad (22)$$

where $\omega_{02} = \sqrt{k_s / (m + m_0)}$ and $\omega_{03} = \sqrt{k_0 / (m + m_0)}$.
 The natural frequency is as follows:

$$\omega_n = \sqrt{-\frac{\omega_{02}^4}{2\omega_c^2} + \omega_{03}^2 + \sqrt{\left(\frac{\omega_{02}^4}{2\omega_c^2} - \omega_{03}^2\right)^2 - (\omega_{03}^4 - \omega_{02}^4)}}. \quad (23)$$

The last expression (Eq. (23)) was verified by a 2D finite element solution (Fig. 14), the maximum difference is 8 %. Despite of the major simplifications the frequencies of the model (Eq. (23)) and that of the 2D problem are close to each other.

The solution for base excitation ($u = u_{g0} \sin(\omega t)$) was also derived, the result is:

$$\bar{D}_{\kappa r} = u_r(x=0, \omega) = \left(\frac{1 - \frac{\omega_{03}^2}{\omega^2}}{\frac{\omega_{02}^2}{\omega^2} \sqrt{1 - \frac{\omega^2}{\omega_c^2}} + \frac{\omega_{03}^2}{\omega^2} - 1} + 1 \right) u_{g0} \frac{1}{1 - \frac{\omega^2}{\omega_c^2}}. \quad (24)$$

The derived expressions were verified by several comparisons to finite element solutions, some of those are presented in Appendix B. The numerical and analytical solution of an axially constrained bar is given below in Fig. 15.

5 Significance of the model

In the previous section we derived an expression for the displacement of the structure subjected to a harmonic base excitation. The amplitude of the steady-state solution is given by Eq. (24). It is an important observation that there are two singular points in the resonance curve. One belongs to the eigenfrequency (when the denominator of

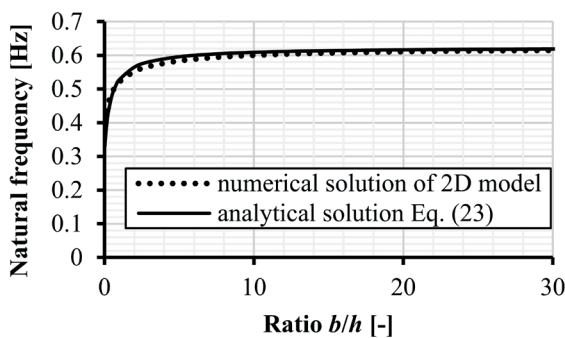


Fig. 14 Natural frequency of the simplified model (Eq. (23)) and 2D model

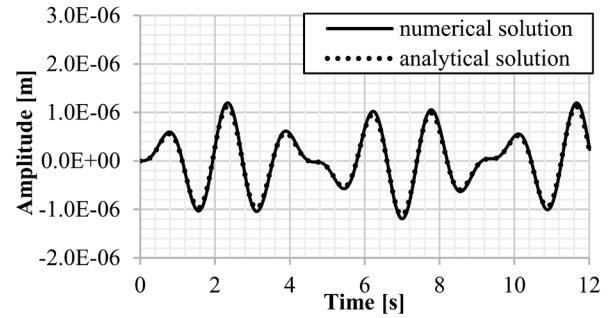


Fig. 15 Verification of the derived expression (Eqs. (11), (13), (17) and (18))

$$(EA = 1810^6 N, \kappa = 55.5 \cdot 10^3 \frac{N}{m^2}, \mu = 1800 \frac{kg}{m}, m = 72267 kg, F_0 = 1, \omega = 4.712 Hz, u_0 = 0, v_0 = 0)$$

the first fraction in Eq. (24) becomes zero), while the second one to the cut-off frequency (ω_c) when the denominator of the second part of Eq. (24) is zero.

Although for real cases, when we have a material damping, and the duration of an earthquake is finite there are no singular points, but definitely there are high peaks on the resonance curve. When the dominant frequency of an earthquake is close to the eigen frequency or to the cut-off frequency it is expected that the response displacement will be very high. Now we investigate the realistic range of the cut-off frequency and natural frequency.

When the frequency is below the cut-off frequency the phase angle is $\phi = 0^\circ$, and there is no energy dissipation in the system, while for higher frequency $\phi = 90^\circ$, there is a loss in energy. If we try to model this behavior with springs, masses and dashpots, we must face the following contradictions. For $\omega < \omega_c$ no dashpot is needed, while for $\omega > \omega_c$ a dashpot must be applied. If we choose one of these, for the other case our modelling will be inadequate.

The importance of the above contradiction of the energy dissipation will be treated in the numerical example.

Eqs. (8), (19) and (4) give the following expressions for ω_c and ω_n :

$$\frac{1}{\omega_c^2} = \frac{h^2 4\rho}{G \pi^2}, \quad (25)$$

$$\frac{1}{\omega_n^2} = \frac{h^2 4\rho}{G \pi^2} + \frac{m 2\sqrt{2}}{G \pi}, \quad (26)$$

which can be rearranged as:

$$\sqrt{G} = \omega_c \sqrt{\frac{4\rho}{\pi^2}} h, \quad (27)$$

$$\sqrt{G} = \omega_n \sqrt{\frac{4\rho}{\pi^2} h^2 + \frac{2\sqrt{2}}{\pi} m}. \quad (28)$$

The circular frequency of a typical earthquake is in the range of 3 Hz $\leq \omega \leq 15$ Hz [19]. The cut-off or the natural frequency is in this range, if:

$$3\sqrt{\frac{4\rho}{\pi^2} h} \leq \sqrt{G} \leq 15\sqrt{\frac{4\rho}{\pi^2} h^2 + \frac{2\sqrt{2}}{\pi} m}. \quad (29)$$

The corresponding curves for different masses (m) (and $\rho = 1800$ kg/m³) are given in Fig. 16.

It can be observed that resonance may occur for realistic soil characteristics. In this range (Fig. 16 grey area) is important to use a model which considers the resonance effect. In [2] this phenomenon was investigated numerically with 2D FE analysis and similar results were obtained.

6 Numerical example

We present 3 numerical examples and the results of our model will be compared to simple spring, mass, (dashpot) systems.

We consider a flat, rigid structure. The total mass is $2m = 720$ t, the width is $2b = 20$ m, and it is resting on a soil layer with a total thickness of $h = 50$ m and shear wave velocity $v_s = 100$ m/s² (Fig. 17(a)).

The parameters of our replacement model for one meter width is calculated by Eqs. (4), (6) and (7) which results in:

$$\overline{EA} = 900 \cdot 10^6 \text{ N}, \quad \mu = 45000 \frac{\text{kg}}{\text{m}}, \quad \kappa = 444132 \frac{\text{N}}{\text{m}^2}, \quad (30)$$

$$m_0 = 900 \cdot 10^3 \text{ kg}, \quad k_0 = 8882643 \frac{\text{N}}{\text{m}}.$$

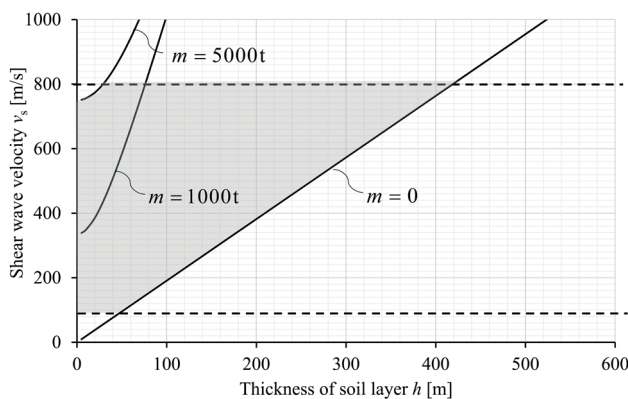


Fig. 16 Critical domain (grey area), where resonance may occur for different masses according to Eq. (29)

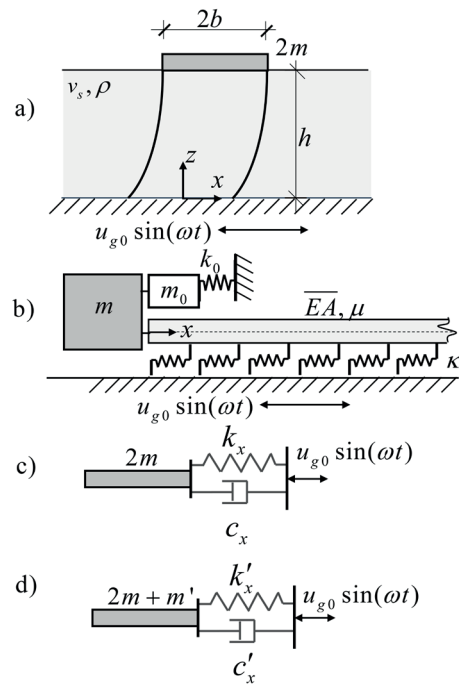


Fig. 17 Models analyzed for base excitation

If the cone model is used, which was developed originally for infinite thickness, it gives zero concentrated mass [4]. The spring constant is determined here in such a way that the static response of the 2D structure and the model is identical. First, for simplicity, the damping is neglected.

Comparisons on the impedance curve are given in Fig. 18. Since the resonance frequency of the spring-dashpot model is different from the real case, the error of the simple spring-dashpot model close to the resonance is enormous. Also note that our model (axially constrained) – using the simple replacement stiffnesses – and the 2D solution give similar answers.

Now we chose a spring-mass model, where the mass was determined to match the resonance frequency. We obtained $m' = 1771214$ kg.

For this model (together with the 2D and our model) the impedance curves are given in Fig. 19. We may observe that although for zero frequency the curves are identical and the resonance points are at the same location the spring model for low frequency overestimates the response while for high frequency underestimates it. More importantly the phase angle is very different. Our model is much better than the spring model (note however that the higher resonances cannot be handled.)

To further show the essential differences between the models two time-history analyses are given for two different harmonic excitations (Fig. 20), one below and one

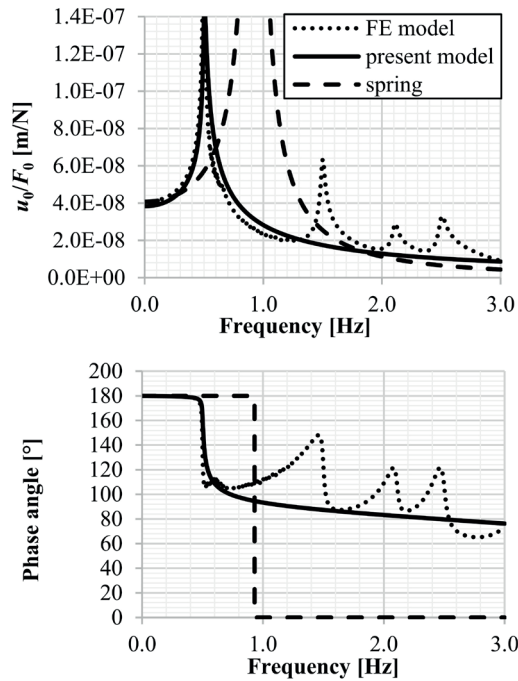


Fig. 18 Impedance curve (steady-state solution) of the different models (Fig. 17(a), Fig. 17(b), Fig. 17(c))

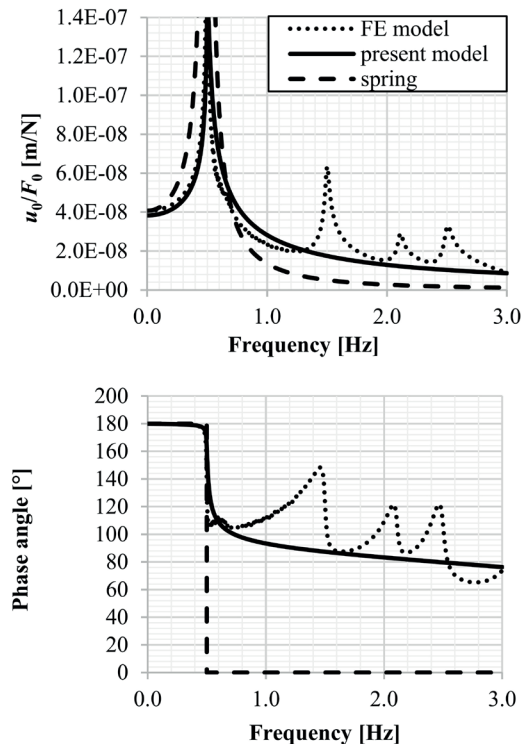


Fig. 19 Impedance curve (steady-state solution) of the different models (Fig. 17(a), Fig. 17(b), Fig. 17(d))

above the cut-off frequency. The results in Fig. 20 clearly show that although our model and the spring-mass model has the same static stiffness and resonance point, their responses are strongly different.

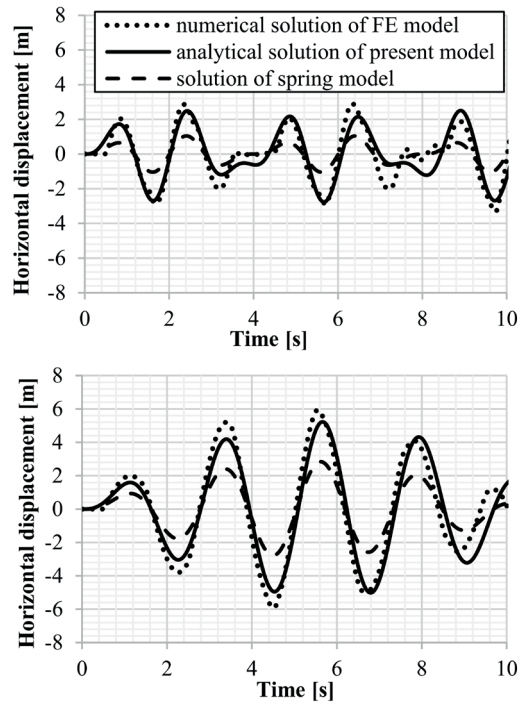


Fig. 20 a) Full solution of the models ($\omega = 4.71 \text{ Hz} > \omega_n = 3.09 \text{ Hz}$), b) full solution of the models ($\omega = 2.5 \text{ Hz} < \omega_n = 3.09 \text{ Hz}$)

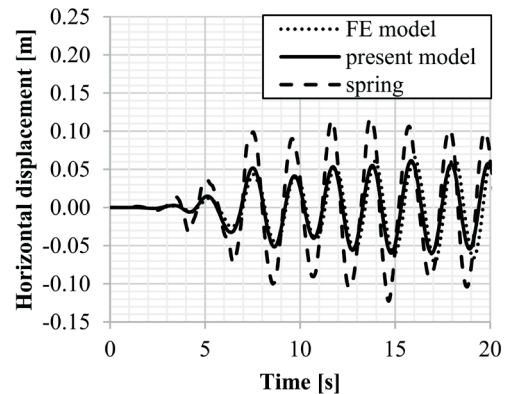


Fig. 21 Solution of the different models for an earthquake record ([19] record no. 32)

Now the resonance for an earthquake record [19] was calculated, the results are shown in Fig. 21. We may have similar conclusions as for harmonic excitation: our new model gives a reasonable response, while the spring model, in spite of matching the static response and the resonance frequency is inaccurate.

In Fig. 22 the impedance curves of the different models with damping can be seen. For the 2D model and our 1D model 5 % material damping is used. With dashed line the impedance of the spring-dashpot model (Fig. 17(d)) is showed, but to reach a similar amplitude curve, 12 % damping ($c'_x = 1878331 \text{ Ns/m}$) had to be used. The dashed-dot line shows the results of a spring-dashpot model

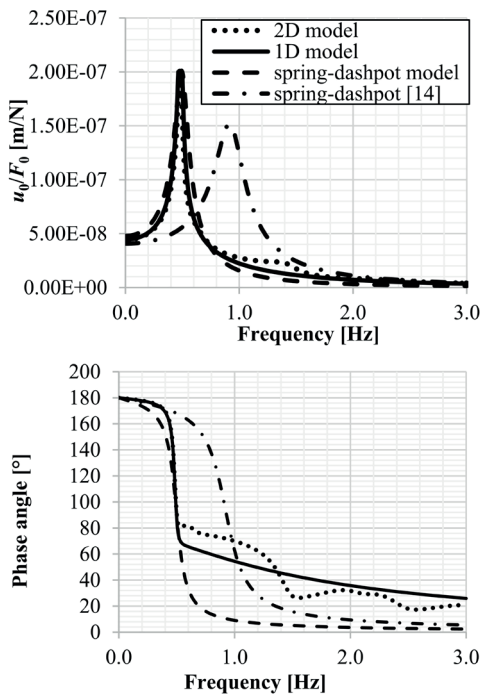


Fig. 22 Impedances with damping

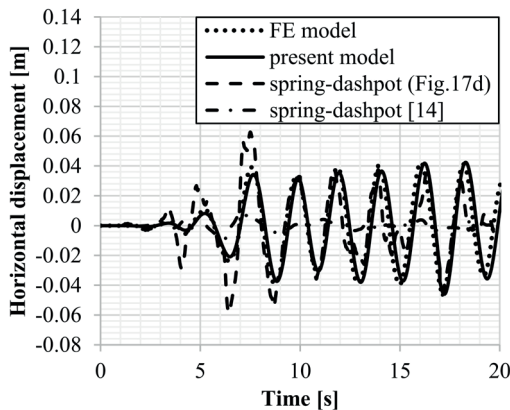


Fig. 23 Solution of the different models for an earthquake record ([19] record no. 32)

(Fig. 17(c)), where the parameters are calculated by formulas in the literature [15]. For the models showed in Fig. 17(a), (b) and (d) the amplitude curves of the impedance function are similar, but the phase angle for the spring-dashpot model is quite different.

The differences in the models are also presented by time-history analysis for an earthquake record [19] in Fig. 23.

7 Conclusions

A rigid structure resting on a finite depth soil layer was investigated. The size of the object resting on the soil influences the behavior of the layer, their interaction was investigated. When the structure is long in one direction the 2D problem can be reasonably well modelled by an axially

constrained bar (Fig. 6), where the bar stiffness (\overline{EA}), mass per unit length (μ) and the coefficient of elastic foundation (κ) depend on the soil parameters and on the stiffness of the soil layer. (It can be shown that the response of bars on elastic foundation with the same cut off frequency $\omega_c = \sqrt{\kappa / \mu}$ and same replacement spring constants $k_s = \sqrt{\kappa \overline{EA}}$ behave identically, i.e. there are only two independent parameters (ω_c, k_s) instead of three ($\overline{EA}, \mu, \kappa$.) In the model a spring (k_0) and a concentrated mass (m_0) must be taken into account, which depend on the size of the foundation. The concentrated mass can be interpreted as the soil which directly moves together with the object. The recommended model can be considered as two submodels connected parallelly: a spring-mass system and a beam on elastic foundation.

The above simplified model subjected to base excitation can be and was solved analytically and the response of the system was analyzed. When the frequency of a harmonic excitation is above the so called cut-off frequency there is a high radiation damping, while when it is below, the radiation damping vanishes. Note that this phenomenon can not be observed on single spring-dashpot systems.

It is recommended that in modelling the soil structure interaction by FE the effect of the soil should be taken into account by the presented model (with a reasonable damping ratio to account for the material damping). This model contains both the possible resonance of the soil-structure system and the cut-off frequency which determines the role of the radiation damping. These phenomena are significant part of the behavior; their negligence (e.g. by using single spring-dashpot supports) may lead to unacceptable errors during earthquake design.

When more complex models (such as the lumped model, Fig. 2) are used, to achieve proper accuracy with a reasonably low number of parameters it is recommended that one of the submodels is an axially constrained bar.

One may argue that the soil cannot be modelled by elastic material laws, not even with high damping coefficient, since their stress-strain curve is highly nonlinear and the hysteretic behavior depends strongly on the size of the strains. We fully agree with these statements, strictly speaking, the above modelling valid only for low strains, where the stresses and strains are in the linear part of the stress-strain curve. Nevertheless, even if we wish to have a reasonable model for higher strains, the model should contain the important phenomena discussed above. To reach both goals, i.e. a model which contains the cut-off frequency (and resonance) and also the nonlinear soil characteristics it seems a good solution if in the above model the stiffness

characteristics (\overline{EA} and κ) are not uniform and the material laws $N = EA\kappa$ and $p = \kappa u$ are not linear (Fig. 6). To develop these material models is not part of this paper.

The presented model takes into account two resonant points between the rigid structure and the supporting soil, the first natural frequency and the cut-off frequency. In the 2D solution there are further resonance points, since in the soil layer higher modes can develop (Fig. 24). These might be taken into account by the combination (serial or parallel) of our simple model, however this is also not the task of this paper.

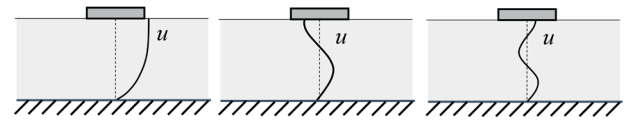


Fig. 24 Higher modes of the soil layer

Acknowledgements

The authors gratefully thank the support of the OTKA 115673 project of the Hungarian National Research, Development and Innovation Office.

References

- [1] Lai, C. G., Martinelli, M. "Soil-Structure Interaction", ALERT Doctoral School, ALERT Geomaterials, Grenoble, France, 2013.
- [2] Pap, Z. B., Kollár, L. P. "Effect of Resonance in Soil-Structure Interaction for Finite Soil Layers", *Periodica Polytechnica Civil Engineering*, 62(3), pp. 676–684, 2018.
<https://doi.org/10.3311/PPci.11960>
- [3] Kausel, E. "Early history of soil-structure interaction", *Soil Dynamics and Earthquake Engineering*, 30(9), pp. 822–832, 2010.
<https://doi.org/10.1016/j.soildyn.2009.11.001>
- [4] Wolf, J. P., Deeks, A. J. "Foundation vibration analysis: a strength-of-materials approach", Butterworth-Heinemann, Oxford, UK, 2004.
- [5] Çelebi, E., Firat, S., Çankaya, I. "The evaluation of impedance functions in the analysis of foundations vibrations using boundary element method", *Applied Mathematics and Computation*, 173(1), pp. 636–667, 2006.
<https://doi.org/10.1016/j.amc.2005.04.006>
- [6] Andersen, L. "Assessment of lumped-parameter models for rigid footings", *Computers and Structures*, 88(23–24), pp. 1333–1347, 2010.
<https://doi.org/10.1016/j.compstruc.2008.10.007>
- [7] Mylonakis, G., Nikolaou, S., Gazetas, G. "Footings under seismic loading: Analysis and design issues with emphasis on bridge foundations", *Soil Dynamics and Earthquake Engineering*, 26(9), pp. 824–853, 2006.
<https://doi.org/10.1016/j.soildyn.2005.12.005>
- [8] Dunn, P. W. "Comparison of cone model and measured dynamic impedance", PhD Thesis, University of Florida, 2010.
- [9] Meek, J. W., Wolf, J. P. "Cone Models for Soil Layer on Rigid Rock. II", *Journal of Geotechnical Engineering*, 118(5), pp. 686–703, 1992.
[https://doi.org/10.1061/\(ASCE\)0733-9410\(1992\)118:5\(686\)](https://doi.org/10.1061/(ASCE)0733-9410(1992)118:5(686))
- [10] Wolf, J. P. "Foundation vibration analysis using simple physical models", Prentice-Hall, Englewood Cliffs, NJ, USA, 1994.
- [11] Wolf, J. P. "Consistent lumped-parameter models for unbounded soil: frequency independent stiffness, damping and mass matrices", *Earthquake Engineering & Structural Dynamics: The Journal of the International Association for Earthquake Engineering*, 20(1), pp. 33–41, 1991.
<https://doi.org/10.1002/eqe.4290200104>
- [12] Wolf, J. P. "Spring-dashpot-mass models for foundation vibrations", *Earthquake Engineering and Structural Dynamics: The Journal of the International Association for Earthquake Engineering*, 26(9), pp. 931–949, 1997.
[https://doi.org/10.1002/\(SICI\)1096-9845\(199709\)26:9<931::AID-EQE686>3.0.CO;2-M](https://doi.org/10.1002/(SICI)1096-9845(199709)26:9<931::AID-EQE686>3.0.CO;2-M)
- [13] Wolf, J. P. "Consistent lumped-parameter models for unbounded soil: physical representation", *Earthquake Engineering and Structural Dynamics: The Journal of the International Association for Earthquake Engineering*, 20(1), pp. 11–32, 1991.
<https://doi.org/10.1002/eqe.4290200103>
- [14] Saitoh, M. "Simple Model of Frequency-Dependent Impedance Functions in Soil-Structure Interaction Using Frequency-Independent Elements", *Journal of Engineering Mechanics*, 133(10), pp. 1101–1114, 2007.
[https://doi.org/10.1061/\(ASCE\)0733-9399\(2007\)133:10\(1101\)](https://doi.org/10.1061/(ASCE)0733-9399(2007)133:10(1101))
- [15] Dobry, R., Gazetas, G. "Dynamic Response of Arbitrarily Shaped Foundations", *Journal of Geotechnical Engineering*, 112(2), pp. 109–135, 1986.
[https://doi.org/10.1061/\(ASCE\)0733-9410\(1986\)112:2\(109\)](https://doi.org/10.1061/(ASCE)0733-9410(1986)112:2(109))
- [16] Hughes, T. J. "The finite element method Linear static and dynamic finite element analysis", Prentice-Hall, Englewood Cliffs, NJ, USA, 1987.
- [17] Hagedorn, P., DasGupta, A. "Vibrations and Waves in Continuous Mechanical Systems", John Wiley & Sons, Chichester, UK, 2007.
<https://doi.org/10.1002/9780470518434>
- [18] Dunkerley, S. "On the whirling and vibration of shafts", *Philosophical Transactions of the Royal Society London (A)*, 185, pp. 279–360, 1894.
<https://doi.org/10.1098/rsta.1894.0008>
- [19] FEMA "Quantification of Building Seismic Performance Factors", Applied Technology Council, Redwood City, CA, USA, Rep. FEMA P695, 2009.

Appendix A: Euler-Lagrange equation of a soil layer

The assumed displacement field is given by Eq. (1), the potential energy of the system is defined by Eq. (2). The Euler-Lagrange differential equation of the system can be derived from the stationary condition $\Pi = \text{stationary}$. Accordingly a small variation of the function will not change the value of potential energy:

$$u \rightarrow u + \eta \delta u \rightarrow \left. \frac{d\Pi(u + \eta \delta u)}{d\eta} \right|_{\eta=0} = 0, \tag{A1}$$

where δu is a kinematically admissible function, which is zero at the boundaries, η is a small number.

The variation of the potential energy:

$$\begin{aligned} \Pi(u + \eta \delta u) = & \int_x \frac{Gh}{2} [u'^2 + 2\eta u' \delta u' + \eta^2 \delta u'^2] \\ & + \frac{G\pi^2}{16h} [u^2 + 2\eta u \delta u + \eta^2 \delta u^2] \\ & - \rho \frac{h}{4} [\ddot{u}^2 + 2\eta \ddot{u} \delta \ddot{u} + \eta^2 \delta \ddot{u}^2] dx. \end{aligned} \tag{A2}$$

The stationary condition is the following:

$$\left. \frac{d\Pi(u + \eta \delta u)}{d\eta} \right|_{\eta=0} = \frac{Gh}{2} \int_x \left\{ \delta u \left[-2u'' + \frac{\pi^2}{4h^2} u + \frac{\rho}{G} \ddot{u} \right] \right\} dx. \tag{A3}$$

This must be satisfied for any δu function, hence we may write:

$$-Ghu'' + \frac{G\pi^2}{8h} u + \frac{\rho h}{2} \ddot{u} = 0. \tag{A4}$$

Eq. (A4) is the Euler-Lagrange equation of Eq. (3).

Appendix B: Solution of the differential equation of the axially constrained bar with an end mass

The differential equation is given by Eq. (3). The general solution can be given as in Eq. (11). The parameter \bar{D} can be derived from the boundary conditions:

$$N(x = 0, t) = F - m\ddot{u}, \tag{B1}$$

where N is the normal force at the end of the bar.

Substituting the material law $N = EA\varepsilon$ into Eq. (B1) results in:

$$EAu'(0, t) = F - m\ddot{u}(0, t). \tag{B2}$$

The parameter can be determined by performing the derivations:

$$\begin{aligned} \bar{EAik}\bar{D} &= F_0 + m\omega^2 \bar{D}, \\ \bar{D} &= \frac{F_0}{EAik - m\omega^2}. \end{aligned} \tag{B3}$$